Comparison of intense-field ionization of diatomic molecules and rare-gas atoms

E. Wells,[1] Merrick J. DeWitt,[2] and R. R. Jones[1]
[1]*Department of Physics, University of Virginia, Charlottesville, Virginia 22904-4714*
[2]*Center for Atomic, Molecular, and Optical Science, Department of Chemistry, University of Virginia, Charlottesville, Virginia 22904-4319*
(Received 23 January 2002; published 24 July 2002)

Strong, short laser pulses have been used to ionize diatomic molecules and rare-gas atoms. Using mixed species targets, intensity-dependent ionization yield ratios have been measured directly for pairs of molecules and atoms with similar ionization potentials. Specifically, ionization rate ratios for homonuclear (N_2:Ar, F_2:Ar, D_2:Ar, O_2:Xe, S_2:Xe) and heteronuclear (CO:Kr, NO:Xe, SO:Xe) molecules have been obtained. Our experimental results are compared to the predictions of several approximate theoretical models. In general, these models fail to accurately describe the detailed differences in the intense laser ionization rates of atomic and diatomic targets.

DOI: 10.1103/PhysRevA.66.013409 PACS number(s): 33.80.Rv, 32.80.Rm, 42.50.Hz, 34.50.Gb

I. INTRODUCTION

Single electron ionization is perhaps the most fundamental process initiated during the exposure of an atom or molecule to an intense laser pulse. It is also one of the best studied. In atoms, the single active electron (SAE) approximation has enabled quantum simulations of strong-field ionization phenomena that reproduce even the most complex energy and angular distribution spectra with high accuracy [1–5]. There have even been recent theoretical successes in describing multiple ionization of atomic targets [6] where the SAE approximation cannot be used. There is, however, growing interest in understanding the ionization behavior of molecules in strong fields, as lasers are being used for diverse applications such as controlling the photofragmentation branching ratio of large molecules [7–9] or as ''soft'' ionizers for mass spectrometry [10–12]. Unfortunately, quantum calculations on even relatively simple diatomic molecules are extremely difficult, and strong-field molecular ionization is generally treated using more approximate multiphoton [13,14] or tunneling [15–17] models.

Early experimental data [18] indicated that the ionization rates of diatomic molecules were essentially identical to those of atomic targets provided the electron binding energies were nearly the same. Thus, approximate formulas that yield surprisingly accurate total ionization rates in atoms, and depend only on the ionization potential (IP) of the target and the laser intensity and wavelength, were expected to predict strong-field ionization rates of molecules as well. More recent observations have challenged this idea. The ionization of O_2 (IP = 12.07 eV) was found to be suppressed, by approximately an order of magnitude, relative to Xe (IP = 12.13 eV) [19,20]. In a similar result, hydrogen molecules were found to be harder to ionize than ''companion'' argon atoms [21]. In contrast, N_2 displayed [19,20] an ionization rate quite similar to the rate of argon, which has a similar IP (see Table I for a listing of target IPs as well as other molecular properties).

What makes some, but not all, diatomic molecules harder to ionize than their companion atoms? Several attempts have been made to explain the available data, particularly for the case of O_2. First, the production of a doubly excited state, via collisions of a rescattered electron and the molecular ion, which then dissociates into two neutral atoms (i.e., dissociative recombination) has been proposed as a mechanism that could suppress the production of O_2^+ [19]. Subsequent measurements [20] show little dependence of the O_2 suppression on the ellipticity of the laser polarization, indicating that the dissociative recombination mechanism is unlikely to be the source of the anomalously low O_2^+ yield. Second, a modified tunneling model that accounts for the two-center potential of a diatomic molecule [23] provides qualitative agreement with the O_2 data, but is unable to explain the magnitude of the suppression [23]. Talebpour *et al.* [21] also consider the orientation of the two-center potential relative to the laser polarization to explain the suppression of ionization in D_2. They calculate an effective charge for incorporation into atomic tunneling theory and include an effective increase in the molecular ionization potential due to the non-negligible Franck-Condon overlap between the field-free ground state and field-free vibrationally excited states of the molecular ion. They achieve good agreement between theory and experiment provided that the correct value of the effective charge is used [21]. Third, a recent investigation of the influence of vibrational motion and field induced changes in bond lengths on the ionization rates of H_2 and O_2 also predicts reduced ionization rates relative to companion atoms of the same IP, but cannot quantitatively account for the observed suppression [24].

The results of two recent calculations, based on very different theoretical models, are in quantitative agreement with the O_2 and N_2 experimental data. Both models suggest general prescriptions for treating the complexities associated with molecular structure in a straightforward way. Guo has introduced a structure correction [25] to a tunneling formula [17]. As in the case of D_2 described above, the observed suppression of O_2 is reproduced, provided the correct parameters for the effective nuclear charge and effective IP are chosen. In the context of this model, the observed absence of suppression in N_2 [20] is explained by the uniform distribution of the outer electrons around the ionic molecular core,

TABLE I. Summary of the target properties. IP is the ionization potential, R_0 is the average internuclear distance, Ψ_{ground} is the ground-state wave function, and HOMO is the highest occupied molecular orbital. The values were taken from Ref. [22]. We were unable to locate polarizability measurements for SO and S_2.

Target	IP (eV)	R_0 (Å)	Cation R_0 (Å)	Polarizability (10^{-24} cm^3)	Ψ_{ground}	HOMO
N_2	15.581	1.098	1.116	1.7403	$^1\Sigma_g^+$	σ_g
F_2	15.697	1.412	1.322	1.38	$^1\Sigma_g^+$	π_g
D_2	15.467	0.742	1.056	0.795	$^1\Sigma_g^+$	σ_g
O_2	12.070	1.208	1.116	1.5812	$^3\Sigma_g^-$	π_g
S_2	9.356	1.889	1.82		$^3\Sigma_g^-$	π_g
SO	10.294	1.481	1.42		$^3\Sigma^-$	π_g
CO	14.014	1.128	1.115	1.95	$^1\Sigma^+$	σ_g
NO	9.264	1.151	1.063	1.7	$^2\Pi$	π_g
Ar	15.764			1.6411		
Kr	13.997			2.484		
Xe	12.13			4.0455		

resulting in an atomiclike potential with an effective nuclear charge of 1.0.

A second model, proposed by Muth-Böhm and coworkers [26] explains the suppression of O_2 as a ''two-slit'' interference effect, arising from emission of electron waves from two distinct centers in the diatomic potential. By adding an interference term [26] to a generalized form of intense-field many-body *S*-matrix theory [27], they are able to correctly predict the suppression of O_2 and its absence in N_2. In the low energy limit where the ionizing electron's de Broglie wavelength is long compared to the internuclear separation, completely constructive (destructive) interference occurs if electron amplitude is emitted from the respective atomic centers perfectly in phase (out of phase). In molecules with symmetric electronic ground-state wave functions, e.g., N_2, the interference is constructive and ionization via ejection of low energy electrons proceeds as if from a single atomic center. On the other hand, in molecules with antisymmetric ground states, e.g., O_2, the interference is destructive, totally suppressing ionization through dominant low energy channels. Indeed, as predicted, recent measurements of above-threshold ionization (ATI) show an absence of low energy electron emission during strong-field ionization of O_2 [28]. Muth-Böhm *et al.* [26] also made a quantitative prediction of ionization suppression of F_2 relative to N_2. Moreover, the interference model predicts ionization suppression in all diatomic molecules with antisymmetric electronic ground states. Recently, the formalism has been generalized to symmetric polyatomic molecules as well [29]. The conclusion of Ref. [29] is that multicentered complex molecules cannot have a higher ionization rate than single centered atoms, since the interference effect can only decrease the total probability for ionization. Indeed, suppressed ionization has been observed in C_6H_6 molecules [11,30]. If suppression due to interference effects is a general phenomenon in molecular ionization, the model provides a useful tool for calculating accurate ionization rates of many molecules.

Motivated by a desire to test these theoretical predictions, we recently reported [31] high precision ratiometric measurements of the ionization rates of N_2, O_2, S_2, and F_2 as compared to atomic targets of similar ionization potentials. Some of our results were at odds with theoretical predictions, particularly with regard to S_2 and F_2. In this paper we provide more details of the previous measurements [31], and report on measurements of four additional species; D_2, CO, NO, and SO. When combined with the previous measurements, we have completed studies of most readily available diatomic molecules.

We report molecular:atomic ionization yield ratios rather than single species ionization probabilities in order to provide more accurate data for comparison with theoretical work in this area. While the individual ionization rates vary by up to eight orders of magnitude over the intensity ranges studied, the yield ratios typically differ by less than a factor of ten over this same intensity range. In addition, our molecular and atomic data are taken under identical conditions, so that the ionization ratios are not particularly sensitive to the fine details of the laser beam spatial mode or its focusing characteristics, and relative intensity calibration between any two species is guaranteed. Therefore, the intrinsic uncertainties in the comparison of experiment and theory for individual species are minimized. Because accurate atomic ionization rates are presumably straightforward to calculate, direct comparison of experimental and theoretical ionization yield ratios should provide stringent tests of calculations of high field molecular ionization. The collective results presented in this paper indicate that an accurate, general, and practical method for calculating intense-laser ionization of diatomic molecules does not yet exist.

II. EXPERIMENTAL METHOD

Measurements of the relative ionization yields of individual targets are challenging since, given the rapid change in the ionization rates as a function of laser intensity, an accurate measurement depends critically on control of the laser intensity. As a result, these experiments are sensitive to small changes in the laser power and alignment. Furthermore, in order to simplify the interpretation of the data, most ion yield measurements are made with an aperture limiting

the volume of the ionization region exposed to the detector [20,32]. As a result, small changes in the position of the laser focus due to both nominal beam alignment and shot-to-shot fluctuations in the position of the laser beam can also have a sizable effect on the measured ionization rates. Instead of concentrating on perfect shot-to-shot and run-to-run control of the laser intensity and spatial position, we have opted for a different approach to reducing the contribution of systematic errors. Introducing the molecular target of interest into the ultrahigh vacuum (UHV) chamber concurrently with a reference atomic target allows high precision determinations of relative ionization probabilities. Since any change in laser intensity or alignment affects both analytes, the reliability of the measurement is enhanced over separate, single target, measurements. While this ratiometric approach is not new for ionization measurements, (see, for example, Ref. [33]) it is particularly useful in cases where small changes in the laser intensity have such large impact. This section describes our experimental technique, with special attention paid to the key issue of sample characterization.

A. Measurement

The experiments are performed using a commercial Ti:sapphire laser that produces 790 nm, 100 fs pulses with an energy of 2 mJ at a repetition rate of 1 kHz. The pulse duration is monitored with a single shot autocorrelator. Pulse attenuation is performed with a half-wave plate and polarizing beam splitter and the subsequent pulses are focused with either a crown glass lens with a 30 cm focal length or a gold mirror with a 5 cm focal length. The maximum intensity of these focused pulses is in excess of 10^{15} W cm^{-2}. For some targets, discussed in Sec. III, the 790 nm pulses are used to pump an optical parametric amplifier (OPA) producing 1365 nm, 80 fs pulses of approximately 150 μJ, also at a repetition rate of 1 kHz. These pulses are focused with the 5 cm focal length mirror to produce a maximum intensity of 10^{15} W cm^{-2}. The absolute intensity of the laser is determined from the threshold for multiple ionization of rare gas targets reported by several other groups [20,34–36]. An alternative intensity calibration is obtained from the measured beam-spot size, energy, and pulse duration. The absolute intensities determined from these two methods generally agree to within a factor of 2 or 3.

The ionization region is longitudinally confined by a 1 mm slit. A two-stage time-of-flight (TOF) spectrometer [37] is used to extract the ions to a chevron microchannel plate detector. While the exact spectrometer geometry changed several times, the bulk of the measurements were made with a 1.3 cm extraction region, a 0.64 cm acceleration region, and a 44.5 cm field-free drift region. Typical spectrometer fields are 1160 V/cm for the extraction region and 760 V/cm for the acceleration region. These fields are strong enough to obtain 4π collection of ions with kinetic-energy releases of less than 0.5 eV. For some species, notably N_2:Ar, measurements were made with several different spectrometer geometries. For example, one configuration used a 5 cm drift region, significantly increasing the collection efficiency of higher energy ions (4π up to $\approx$2.5 eV). However, none of the spectrometer changes had a significant impact on our results. The microchannel plate signal is amplified and single ion events are recorded with a multichannel scalar (MCS). The MCS is capable of counting multiple events per trigger with a pulse pair resolution of 20 ns; however, the sample pressures are adjusted to ensure a count rate of approximately one event per trigger or less for all masses at all times. The TOF resolution $m/\Delta m$ is approximately 200. A sample TOF spectrum of a mixed CO and Kr target is shown in Fig. 1.

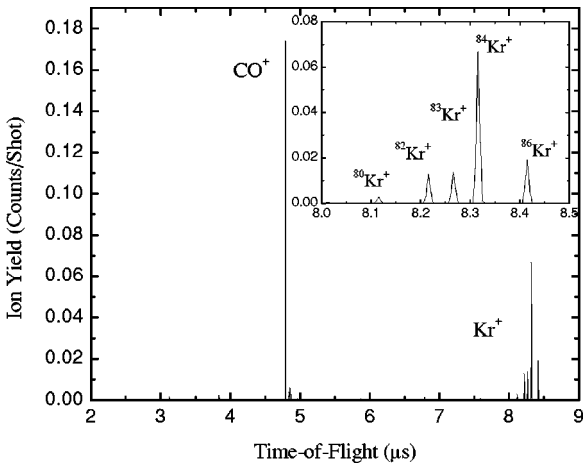

FIG. 1. A typical time-of-flight spectrum showing CO^+ and Kr^+ ionized by 100 fs, 790 nm laser pulses at an intensity of 5.3 $\times 10^{13}$ W/cm^2. Note the isotopic resolution on the Kr^+ peaks.

At each laser intensity, data are collected for anywhere from $\sim 10^5$ to 10^7 laser shots. Multiple measurements at each intensity were made to confirm the reproducibility of the results. After baseline and background subtraction (usually negligible) the ion yield for each m/q is determined by numerical integration. This yield is then divided by the number of laser shots and by the partial pressure of target gas. In this manner, the ionization probability is determined for each target species in units of counts/(shot torr). Runs with over 1 count/shot for any species are discarded to avoid any counting problems. The ratio of molecular to atomic ionization is determined by dividing the ionization yields for the individual species. Our data can be most easily compared with the data of Guo *et al.* [20], who also measured the yield in units of counts/(shot torr) (see Fig. 1 in Ref. [31]). Only the ratio can be reliably compared, however, since differences in the ionization volume lead to differences in the yield even when the partial pressures of the different experiments are taken into account.

While single ionization is by far the dominant channel observed, at higher intensities the double ionization and molecular fragmentation channels are non-negligible. For the data presented here, these channels are handled in one of two ways. In most cases, the fragmentation and double ionization channels are simply added to the single ionization yield. The resulting data then represent the ratio of total molecular ionization to total atomic ionization. In the cases of S_2 and F_2, however, there are small difficulties in determining the origin of the molecular fragment channels. Simultaneous measure-

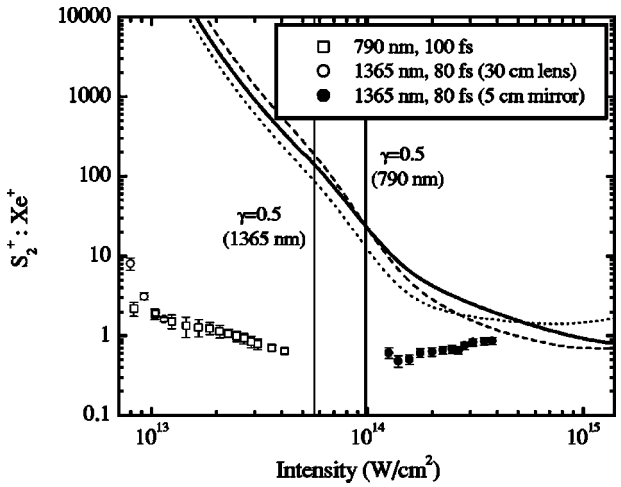

FIG. 2. The measured ratio of S_2^+ to Xe^+ plotted with the predictions of ADK theory as a function of laser intensity. Three ADK calculations are shown: 1365 nm, 80 fs pulses focused with a 5 cm mirror (solid line) and a 30 cm lens (dotted line); 790 nm, 100 fs pulses focused with a 30 cm lens (dashed line). Also included in the spatial averaging calculation is the measured beam diameter for each run. The two vertical lines mark the intensities where the value of the adabaticity parameter (γ) is 0.5 for each of the measured wavelengths. Tunneling theory is expected to be valid to the right of these lines. The measured S_2^+:Xe^+ ratio remains relatively constant over the range of intensities measured, while the calculated ratio changes by several orders of magnitude.

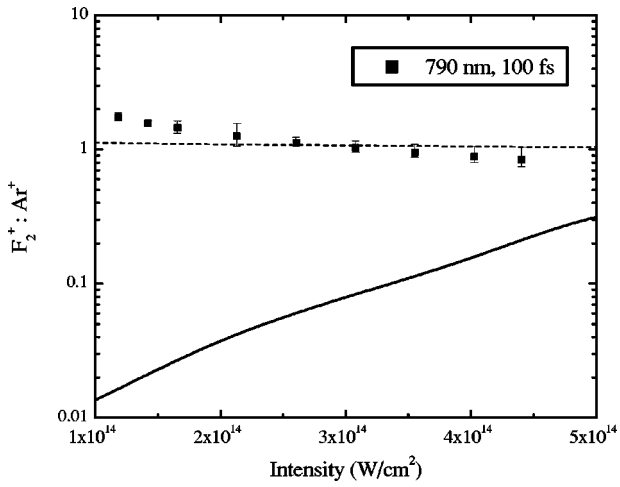

FIG. 3. The ratio of F_2^+ to Ar^{n+} as a function of laser intensity. F_2 is not suppressed compared to its atomic counterpart. The asymmetric error bars reflect the uncertainty in the origin of F^+ fragments, which were added to the F_2^+ yield, but might have originated from HF contamination in the UHV chamber. The dashed line is the prediction of an ADK calculation, similar to those shown in Fig. 2. The solid line is the prediction of the interference model for 200 fs, 800 nm pulses, as estimated from the figures in Ref. [26].

ment of Xe and S_2 is complicated by the overlap of the TOF peaks associated with $^{128}Xe^{2+}$ and $^{32}S_2^+$. The double ionization rate of ^{128}Xe, however, can be inferred from a measurement of $^{132}Xe^{2+}$ and the known isotopic ratio ($^{128}Xe/^{132}Xe = 0.0714$) since $m/q = 66$ is well separated from $m/q = 64$ in our spectrometer. Similarly, S^+ ions formed during the fragmentation of S_2 overlap with O_2^+ ions due to residual oxygen in the chamber, and it is therefore difficult to determine a S^+ yield. In this case, uncertainty in the fragmentation yield is reflected in the error bars on Fig. 2. When F_2 is introduced to the chamber, it reacts with small amounts of residual water and/or hydrocarbons to produce HF. While this contamination is small relative to the amount of F_2, it leads to uncertainty in the origin of F^+ ions. Again, this uncertainty is reflected in the error bars of Fig. 3. It should be emphasized that the primary sources of error in our results arise from statistics (particularly at low intensities) and the uncertainty in the determination of the partial pressures ($\sim 5\%$) and not from double ionization and fragmentation issues. The error bars were calculated from the uncertainties discussed above, and then compared to the scatter in the data from multiple measurements. The larger error from the two methods is reported.

For most of the targets investigated in this work, the effective upper intensity limit of the measurement is the point where the partial pressure can no longer be kept low enough to ensure a counting rate below 1 count/shot for each species. For D_2 and N_2 targets, with IPs greater than 15 eV, higher intensities are accessible. In these cases, an estimate of the double ionization contribution to the total ionization is necessary to determine the correct ratio of molecular to atomic ionization. Given the direction of the laser polarization, the extraction field, the overall efficiency of the microchannel plate (MCP) detector, and the pulse-pair resolution of the MCS, the probability of detecting *both* ionic fragments from a single double ionization event is quite low. In addition, there are dissociative single ionization channels that are experimentally indistinguishable from double ionization in our data. Accordingly, we did not divide the measured D^+ or N^+ yield by a factor of 2.

In the D_2:Ar experiment, another approach is used to extend our measurements to higher field strengths. At intensities below 8×10^{14} W cm^{-2}, the partial pressure of each target gas can be measured at levels low enough to individually count pulses for all ion channels. Above that intensity, the D_2^+ and Ar^{2+} channels are measured using the MCS but the ratio of D^+:D_2^+ and Ar^{2+}:Ar^+ is determined from the TOF signal after averaging over 64 000 shots on a digital oscilloscope. In contrast to the MCS counting technique, when analyzing the oscilloscope data the yield of the D^+ channel is divided by 2, since there is no instrument dead time and both ions contribute to the analog signal. This procedure allows us to perform measurements up to an intensity of 1×10^{15} W cm^{-2}.

B. Sample preparation and characterization

The ionization experiments are carried out in an UHV chamber with a base pressure of $\approx 2 \times 10^{-10}$ torr. The chamber is pumped by a 1000 l/s turbomolecular pump. Residual water vapor is the main contribution to the chamber base pressure in most cases, along with small amounts of hydrocarbons. Both of these contaminants can be reduced to negligible levels by baking the chamber, leak valves, and gas

lines. Unless otherwise noted, the background chamber pressure was sufficiently low during data collection to have no measurable effect on our results.

Targets that are gaseous at standard temperature and pressure are introduced by leak valves into the chamber. Separate leak valves are used for each analyte to maintain controllable leaks equivalent to a change in the partial pressure of the chamber of 1×10^{-10} torr. Sample partial pressures are measured with a quadrupole mass spectrometric residual gas analyzer (RGA) [38] and corrected for electron impact ionization cross section [39–44]. The 70 eV electron impact ionization of the RGA can also result in dissociative ionization of some molecular species. These yields are accounted for in the RGA scan by adding them to the parent ion yield.

Since S_2 molecules are not in the gas phase at STP, they require a different procedure for sample introduction. Bulk sulfur has a high vapor pressure, but is predominantly composed of S_8 at temperatures below $\approx$1000 K [45,46]. We produce S_2 by heating iron pyrites to roughly 350 K and allowing the vapor to effuse into the UHV chamber through a 1 mm pinhole. The pinhole is not aligned with either the RGA or the ionization region so that measured RGA and TOF signals are due to diffuse background S_2 present in the chamber, and not from a S_2 beam. The pyrite oven is differentially pumped with a 70 l/s turbo pump. The pumping speed on the oven region can be varied by means of a valve on the mouth of the turbo pump. Variation of the temperature of the pyrite oven or the pumping speed (or both) allows the S_2 partial pressure to be adjusted from approximately 10^{-9} torr to 10^{-6} torr.

The granular composition of the FeS_2 leads to a significant increase in the water vapor present in the UHV chamber. As the pyrite is heated, we observe SO as well as S_2 production, presumably due to a reaction between the FeS_2 and background H_2O. The amount of SO in the UHV chamber slowly decreases over the period of about a week. Taking advantage of this opportunity, ionization measurements of SO targets are made while the pyrite sample is ''fresh.'' The SO partial pressure remains essentially constant over the duration of an ionization measurement, as is verified by RGA measurement at frequent intervals. The S_2 ionization measurements are not made until the pyrite has been heated for at least several days, and the H_2O and SO levels have been considerably reduced.

C. Consistency checks

Despite the robust nature of the ratiometric technique, the data will be compromised if considerable care is not taken during the experimental process. Key sources of potential problems include (1) misalignment of the ionization region with respect to the ion extraction aperture, (2) nonuniform detection efficiency of the different ion species, (3) uncertainty in the determination of the partial pressure by the RGA, (4) the presence of multiple gas targets with identical m/q ratios, and (5) counting problems associated with pulse pileup at high detection rates. In this subsection, we describe several procedures and consistency checks that are performed to minimize errors in the data collection and analysis.

1. Alignment of laser focus with ion extraction aperture

The relative position of the ionization region and the limiting aperture on the spectrometer entrance determines which part of the laser focal volume is interrogated by the spectrometer. When using the 5 cm mirror to focus the beam, the ionization region is visually aligned with the spectrometer entrance while the chamber is at atmospheric pressure. Proper positioning of the mirror is facilitated by the plasma spark that is created when the mirror is used to focus the laser in air. When using the lens to focus the laser light, the lens position was systematically adjusted until a maximum signal rate was obtained for a given pressure.

A small misalignment of the laser focus and extraction aperture can lead to a significant decrease in ionization signal in our experiment or others with similar spectrometer geometries. As a result, an ionization yield ratio obtained from two single species measurements is extremely sensitive to slight relative changes in the laser focus position and/or size between data runs. Because the ionization yield ratios of all species studied have a relatively weaker laser intensity dependence, the ratiometric measurement technique should be insensitive to any small changes in the laser focus during a dual species run. This assumption has been explicitley tested for N_2:Ar ionization yield ratio measurements by intentially moving the focusing lens to affect the ionization signal. We find that while moving the laser focus away from the center of the slit greatly decreases the overall ionization rate, and enhances the contribution of molecular fragments with high kinetic energy release relative to the primarily thermal distribution of atomic targets, the ratio of N_2^+ to Ar^+ is not strongly affected. We conclude that the ratiometric technique is indeed largely insensitive to alignment problems of this type, particularly at intensities where single ionization is the dominant process.

2. Ensuring uniform detection efficiency for different species

The approximate detection efficiency for single ion events is given by the product of the open area ratio of the microchannel plates and the transmission of the two electroform meshes used in our spectrometer. For this ratiometric measurement, however, having the same detection efficiency for different ion species is the main concern. Uniform detection efficiency of all ions is ensured by accelerating all ions to greater than 4 kV before impacting the first MCP. The ratio of Xe^{2+}/Xe^+ is measured as a function of the lower level discriminator setting on the MCS and measurements are conducted with a discriminator setting well within the region in which the measured Xe^{2+}/Xe^+ ratio is constant. While velocity effects have been observed [47,48] in the analog gain of microchannel plates, it has been demonstrated that for sufficiently high energy ions uniform pulse height distributions, and therefore detection efficiencies, can be achieved even if the ion velocity is not uniform [49–52]. We also note that the extraction voltage of the spectrometer is set high enough that most high energy ion fragments pass through the entrance slit of the spectrometer and are collected. Measurements with different spectrometer geometries, discussed earlier, indicate that the difference in detection solid angle for

dissociating molecules with high kinetic energy release and atomic targets with thermal energies is negligible.

3. Target partial pressure measurements

The RGA determination of the partial pressures was checked by preparing a gas mixture of argon and N_2 similar to those used in earlier experiments [19,20]. Ar (99 torr) and N_2 (156 torr) were combined in a tank which was then filled to a total pressure of 2580 torr with helium, resulting in a 0.043:0.067:1 mixture of $Ar:N_2:He$. The gas mixture was leaked into the chamber and the $Ar:N_2$ ratio correctly reproduced with RGA measurement (to within 4%), confirming the validity of these pressure measurements. This mixture also allowed us to controllably introduce a much lower pressure of Ar and N_2 to explore higher ionizing intensities. A similar procedure was followed with Ar and D_2, with similar results. The F_2 sample is a 5% mixture in He obtained commercially and also verified by RGA measurement. RGA analysis of the chamber is done before and after the ionization measurements, to ensure that the target pressure remains stable over the course of the measurement. The error in each partial pressure measurement is estimated from the fluctuation in the RGA measurement and the uncertainty in the 70 eV electron impact cross section [39–44].

4. Species with identical m/q ratios

Since both the TOF and RGA measurements are mass spectrometry methods, only the m/q of a species can be conclusively determined. Our treatment of the overlap of $^{32}S_2^+$ and $^{128}Xe^{2+}$ in the $S_2:Xe$ experiment is discussed in Sec. II A. Similarly, SO_2 and S_2 both have a mass of 64 amu, and are indistinguishable in our TOF spectra. When the FeS_2 oven is used as a source, TOF peaks at 48 amu and 64 amu are observed. We attribute these to nondissociative ionization of SO and S_2, respectively. However, production of SO_2 in the oven (through a reaction with residual H_2O) and its subsequent fragmentation could produce similar TOF features. To check our assignment, we introduced pure SO_2 into the chamber and compared its ionization-fragmentation TOF spectrum to that obtained using the FeS_2 oven (see Fig. 4). The two results are considerably different. Even at low intensities, pure SO_2 readily fragments into S^+ and SO^+ ions in approximately equal amounts. No peak indicating the production of SO_2^+ is seen. Alternatively, at the same intensity, the spectra from the pyrite source show no signs of S^+. We conclude that the pyrite oven produces S_2 and SO, but negligible amounts of SO_2. Therefore, the 64 amu peak we observe with the pyrite source is indeed due to S_2^+ molecular ions.

5. Hardware counting limitations

Counting problems are avoided primarily by controlling the partial pressures of the targets so that the counting rate does not exceed 1 count/shot for any individual species. When a counting rate of greater than or equal to 1 count/shot is measured, the run is discarded. The bin size on the MCS is 5 ns, and the minimum pulse-pair resolution is 20 ns. The spectrometer geometry and extraction fields are chosen to be high enough that a uniform detection efficiency for all ions is achieved, but also low enough that the width of a typical m/q peak covered several MCS bins. Therefore, some peaks, especially if they contain many isotopes, have a temporal width that is several times greater than the 20 ns pulse-pair resolution of the MCS (see Fig. 1). In these cases, the 1 count/shot restriction is sufficient. If, however, the peak width is limited to only a few 5 ns bins, then a more severe restriction (sometimes as low as 0.25 counts/shot) is imposed. In addition to these critera, determined after the data are collected and analyzed, there are several useful online indications of counting problems. When the experimental counting rate exceeds the pulse-pair resolution of the MCS, the m/q peak becomes heavily weighted to shorter flight times. The shape of a peak, therefore, is a good test of the counting efficiency of the system. The MCP signal is also monitored by a digital oscilloscope averaging many thousands of shots. A difference between the ratio observed on the oscilloscope and that obtained with the MCS indicates that the data have been corrupted by counting problems. In these cases, the partial pressure in the chamber is adjusted and the data are retaken. These additional checks, beyond the

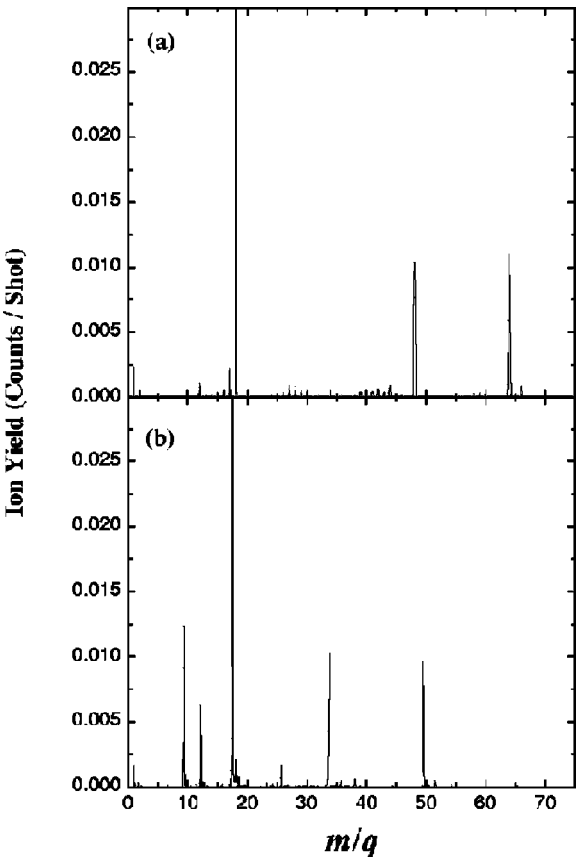

FIG. 4. A comparison of the TOF spectrum produced with 790 nm, 100 fs pulses at 5×10^{12} W/cm^2 by (a) heating FeS_2 and (b) leaking SO_2 into the chamber. SO_2 appears to completely fragment, even at relatively low laser intensities, and no significant peak at $m/q=64$ is observed in the TOF spectrum observed from the SO_2 sample. Also, there is no hint of S^+ from the FeS_2 source, indicating that SO_2 production from the pyrite oven is negligible.

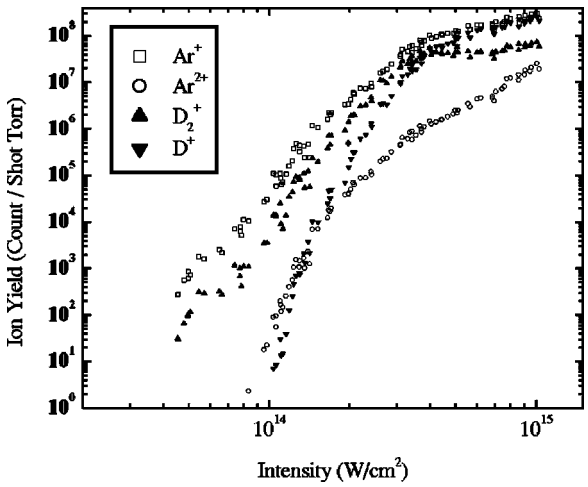

FIG. 5. Ion yield in units of counts/(shot torr) as a function of laser intensity for simultaneously measured D_2 and Ar.

strict 1 count/shot limit, ensure that the experimental results do not suffer from counting errors.

III. RESULTS AND DISCUSSION

Our raw data for the D_2:Ar measurement are shown in Fig. 5. The data taken with the MCS and the MCS-oscilloscope combination, described in Sec. II A, merge together smoothly. The various yields change by nearly eight orders of magnitude over the laser intensities measured, illustrating the difficulty for any detection scheme employed in these measurements. While the D_2 and argon targets are measured simultaneously in our case, it is easy to see that a small shift in intensity for one of the curves could result in a quite different ionization ratio for the two targets. As noted previously, the ratiometric method reduces or eliminates systematic errors due to uncertainties both in intensity and spatial alignment of the laser.

A. F_2:Ar

As noted in the Introduction, previous comparisons of intense-laser ionization yields, N_2 to Ar and O_2 to Xe, indicate that while some molecules (e.g., N_2) do, in fact, ionize at the same rate as companion atoms with the same IP, others (e.g., O_2) behave quite differently. Our yield ratio determinations for N_2:Ar and O_2:Xe confirm the results of the previous experiments [31]. As discussed in Sec. I, two theoretical models accurately predict ionization suppression of O_2 and its absence in N_2. In an attempt to test the direct and indirect predictions of these two models, we measured yield ratios for several other atomic/diatomic pairs as described below.

An explicit prediction of the interference model [26] is that F_2, with its singlet electronic ground state and antisymmetric wave function, should be considerably more difficult to ionize than N_2 or argon, which have nearly identical IPs. Proponents of the structure model [25] argue that ionization of N_2 is not suppressed because the outer electrons are uniformly distributed around the molecular core, resulting in an effective nuclear charge of approximately 1.0. In this scenario, F_2, with its antisymmetric wave function, would be expected to exhibit some suppression, since the ionized electron would be exposed to an effective nuclear charge of greater than 1.0. The yield ratio shown in Fig. 3 indicates that F_2 has essentially the same ionization rate as Ar and N_2 (recall that the N_2:Ar ratio is on the order of unity at all intensities). Therefore, our results for F_2 are clearly at odds with both theoretical models.

B. S_2:Xe

Since F_2 does not show the predicted ionization behavior, one might wonder if the suppression of ionization in O_2 is a special case, or if it is a more general phenomenon that occurs in other molecules. When looking for other targets that might exhibit ionization suppression, S_2 is an obvious choice because of its similar electronic structure to O_2. While both O_2 and S_2 have triplet, antisymmetric ground states, the IP of S_2 is only 9.365 eV, almost 3 eV lower than O_2 or Xe. Using a very simple Ammosov-Delone-Krainov (ADK) or Perelomov-Popov-Terent'ov (PPT) tunneling model, one would expect that the ratio S_2^+:Xe^+ would be much greater than 1.0. Our experimental results, along with ADK calculations, are shown in Fig. 2. The measured ratio near unity indicates, that, like O_2, ionization of S_2 is strongly suppressed.

We note that for 790 nm pulses significant ionization of S_2 occurs at intensities where tunneling theory is not strictly valid. Conventionally, an experiment is considered to be in the tunneling regime if the Keldysh adiabaticity parameter [15]

$$\gamma = \frac{2\omega_0}{\omega_t} = \frac{\omega_0\sqrt{2I_p}}{E_0} \ll 0.5, \tag{1}$$

where ω_0 is the laser frequency, ω_t is the tunneling frequency, I_p is the ionization potential, and E_0 is the electric field strength of the laser pulse, all in atomic units. This parameter, developed for atoms, is still relevant for diatomic molecules; however, some adjustments are required for more complex species [53]. Due to counting rate restrictions, our measurements with 790 nm laser pulses are limited to the $\gamma > 0.5$ ''multiphoton'' regime. However, by using 1365 nm, 80 fs pulses from an OPA, we are able to determine the ionization ratio in the ''tunneling'' regime, $\gamma < 0.5$, as well. As shown in Fig. 2, the measured S_2:Xe ratio is essentially independent of wavelength. Clearly the molecular ionization suppression phenomenon cannot be classified as an exclusively tunneling or multiphoton-ionization effect.

Sulfur dimers are somewhat unusual in that their average internuclear distance is quite large in comparison to the other molecular targets examined (see Table I). In the interference model [26], this is a key parameter, since the generalization of the intense-field many-body *S*-matrix theory (IMST) [27] from the atomic to the molecular case includes an interference term in the IMST molecular ionization rate. The interference term for an antibonding orbital (I_{AB}) is given by

TABLE II. The calculated values of $\sin^2[(\vec{k}_N\cdot\vec{R})/2]$ for the electron energies of the first few above threshold ionization (ATI) peaks for O_2 and S_2. In this calculation, the laser wavelength is 800 nm, and the intensity is 2.65×10^{14} W cm^{-2}, an intensity where the single ionization channel is nearly saturated for both O_2 and S_2 targets.

	O_2	S_2
ATI 1	0.03	0.32
ATI 2	0.17	0.57
ATI 3	0.29	0.75
ATI 4	0.41	0.87

$$I_{AB}=4\sin^2\left(\frac{\vec{k}_N\cdot\vec{R}}{2}\right), \tag{2}$$

where $\vec{k}_N$ is the momentum of the ionized electron after absorbing N photons $[k_N^2/2=N\omega_0-(U_p+I_p)$ where U_p is the ponderomotive energy] and $\vec{R}$ is the internuclear coordinate [26]. For a bonding orbital, $\sin^2[(\vec{k}_N\cdot\vec{R})/2]$ is replaced by $\cos^2[(\vec{k}_N\cdot\vec{R})/2]$. When $k_NR\ll\pi$, the interference is totally destructive (constructive) for antibonding (bonding) orbitals, irrespective of the angle of electron emission relative to the internuclear coordinate. For larger values of k_NR, the interference is constructive at some emission angles and destructive at others for both bonding and antibonding ground states. In this case, the total ionization yield is essentially independent of the ground-state symmetry, but the angular distributions of ejected electrons are distinctly different. Since k_N increases with ATI order, the observability of ionization suppression for antisymmetric orbitals depends greatly on the number of ATI channels for which the condition $k_NR\ll\pi$ is satisfied, and on the relative contribution of these low order channels to the total ionization yield. The large value of $|R|$ for S_2 indicates that, in comparison to O_2, fewer ATI orders satisfy the destructive interference condition (see Table II). Therefore, assuming that the fractional contribution of the low energy electrons to the total yield is similar in S_2 and O_2, one would expect ionization suppression to be *less severe* in S_2 than in O_2. Comparing the relative amounts of "suppression" between S_2 and O_2 is complicated by the fact that S_2 has a lower IP than xenon. In the tunneling region, the S_2:Xe data are between two and ten times lower than the prediction of the ADK model, and at lower intensities they differ by several orders of magnitude, as shown in Fig. 2. In comparison, the O_2:Xe ratio (see Fig. 1 of Ref. [31]) is between 0.1 and 1 over the entire intensity range measured. The differences between the measured yield ratios and the ADK predictions indicate that the suppression of ionization in S_2 is *more severe* than in O_2.

C. D_2:Ar

Hydrogen molecules, while much simpler than the multielectron targets discussed to this point, have the same ground-state configuration and a similar IP to N_2. Unlike N_2 [31], however, the ionization yield from hydrogen molecules has been reported to be substantially suppressed relative to Ar [21]. Our results, shown in Figs. 5 and 6, are consistent with earlier experimental results [21], showing a significant amount of suppression. Our measurements are performed with D_2 rather than H_2 to simplify the assignment of the source of ionization fragments in the TOF spectrum. At laser intensities below ionization saturation for either species the measured D_2^+:Ar^+ ratio ranges from 0.1 to 0.25. Initial attempts to explain this suppression [21,23] focused on the orientation of the molecular axis with respect to the laser polarization. In a more recent paper [24], the effect of the external field on the vibrational overlap between the neutral and ion states is examined. While both predict suppressed ionization of H_2 (or D_2) relative to argon, neither of these models satisfactorily accounts for the observed magnitude of the suppression.

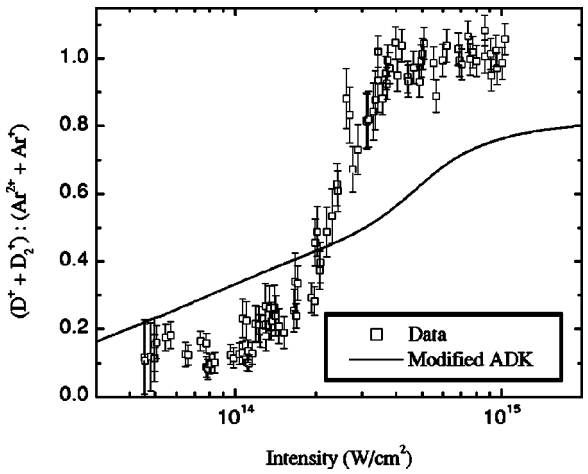

FIG. 6. The ratio of molecular to atomic ionization as a function of laser intensity for a mixed D_2 and argon target. Both single and double ionization of argon are included. The contribution of D^+ fragments to the molecular ionization is accounted for using the method described in Sec. II A.

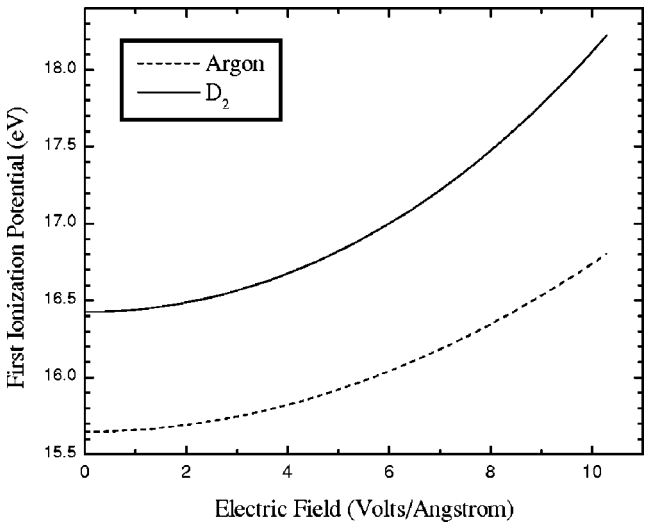

FIG. 7. The calculated ionization potentials of argon and D_2 as a function of applied electric field as described in the text.

We have taken an approach similar to that of Saenz [24] and calculated field-dependent effective ionization potentials for atomic and molecular species. These are then input as intensity-dependent parameters in ADK tunneling theory [17]. The sparse state space of the hydrogen dimer made the D_2:Ar ratio the best test case for this model calculation. Neutral hydrogen energies, in the presence of the laser field, are determined via coupled-cluster theory with GAUSSIAN 98W [54]. Single and double excitations are included in the correlation-consistent quadruple ζ calculation. The hydrogen ion energies are determined with the same basis set via self-consistent Fock theory. The IP is defined as the difference between the ionic and neutral energies as a function of laser intensity. In order to simulate a ''vertical'' transition from neutral to ionic molecular species, in all of the calculations the internuclear separation is fixed at the peak of the vibrational wave function for the field-free molecular ground state. The hydrogen energies were calculated for fields aligned both parallel and perpendicular to the internuclear axis. An ensemble IP is then determined as the average of the IPs in the parallel and perpendicular configurations with a statistical 2:1 weighting of perpendicular:parallel orientations. A zero-point correction of 0.192 eV was applied to the neutral energy. The same calculation was performed for Ar, Ar^+, and Ar^{2+} . The first and second field-free IPs of argon were determined to be 15.65 and 27.46 eV, respectively. These are 0.7% and 0.6% below the experimental values of 15.759 and 27.63 eV, respectively.

The resulting field-dependent IPs, shown in Fig. 7, are incorporated into the ADK tunneling theory [17] to produce ionization rates, which are then temporally and spatially integrated over the focus conditions of the experiment. The results, shown in Fig. 6, reproduce some of the gross features of the data. There are, however, noticeable differences, such as the saturation of the calculation at a value near 0.8 instead of 1.0, and the sharper slope of the data in the region around 2.5×10^{14} W/cm^2. As a consistency check, the Ar^{2+}:Ar^+ ratio has also been calculated and compared to the data. Up to a small uncertainty in the absolute intensity, and considering the inability of the model to account for simultaneous rather than sequential double ionization, the modified ADK calculation reproduces the atomic ionization data quite well. Apparently, the differences between theory and experiment in Fig. 6 are due, primarily, to our inability to estimate accurate molecular ionization rates.

It would be difficult and perhaps not particularly illuminating to extend this modified ADK approach to other species we have studied. First, the calculation of intensity-dependent ionization potentials for other molecules, such as N_2 or O_2, is problematic, as the variational approach employed for D_2 cannot easily deal with field-induced curve crossings in larger molecules. Second, the rather large difference in equilibrium internuclear distance for D_2^+ and D_2 results in a significant difference in the vertical and ground-state IPs. As a result, the effect of the field-dependent IP is likely to be more pronounced in hydrogen than in other molecules. In short, while the results of our model show some qualitative agreement with the data it, like several others before, fails quantitatively. We note that calculations of the field-dependent Franck-Condon overlap integrals would be more realistic than our vertical IPs. In fact, the effect of the vibrational motion on the ionization rate of hydrogen molecules has been studied [24] and the Franck-Condon factors have recently been incorporated into the IMST framework for N_2 [55]. In general, however, calculations of the field-dependent vibrational overlap between the neutral and ionic molecular species are quite difficult to obtain.

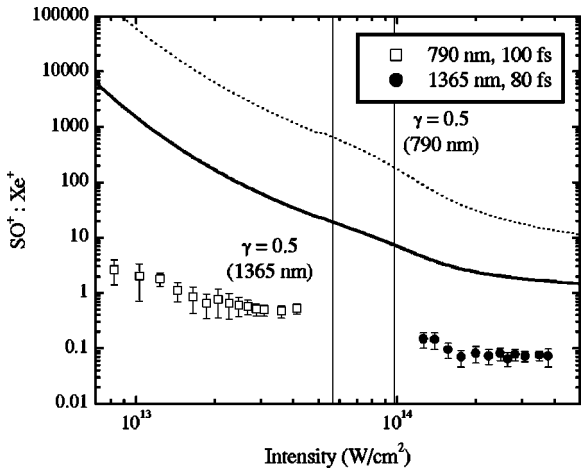

FIG. 8. The measured ratio of SO^+ to Xe^+ as a function of laser intensity along with the predictions of ADK theory. Two calculations are shown: 1365 nm, 80 fs pulses focused with a 5 cm mirror (solid line); and 790 nm, 100 fs pulses focused by a 30 cm lens (dashed line). As in Fig. 2, the vertical lines mark the intensities where $\gamma=0.5$ for the indicated wavelengths.

D. Heteronuclear targets

Sulfur monoxide, while lacking the symmetry of a homonuclear diatom, has much the same electronic structure as O_2 or S_2. Measurements of the SO:Xe ionization ratio, shown in Fig. 8, reveal that SO is quite difficult to ionize, and that the suppression seen in S_2 and O_2 also extends to heteronuclear species. As with S_2, the suppression persists at higher wavelengths as well. Since SO has a higher IP than S_2 (10.294 and 9.356 eV, respectively), it is not unexpected that the values of SO^+:Xe^+ are lower than the corresponding S_2 results. Perhaps a better way to examine the amount of suppression is to examine the difference between the measured ratio and the ratio predicted by a tunneling calculation, since the tunneling ratio theoretically accounts for the difference in IP [56]. At an arbitrarily selected value of 2×10^{14} W/cm^2, the SO^+:Xe^+ ratio is approximately 30 times smaller than the prediction of the ADK model. The same value for the S_2^+:Xe^+ ratio is around 6.4. Thus, in this comparison, SO is $\sim5\times$ harder to ionize than S_2 if the difference in IP is taken into account.

Carbon monoxide is a singlet heteronuclear molecule with a relatively high IP (14.014 eV). We have compared it to krypton, which has a nearly identical IP (13.997 eV). Electronically, CO is quite similar to H_2 (D_2) or N_2. The CO:Kr results are shown in Fig. 9. The structure around 2.5×10^{13} W/cm^2 is believed to arise from the knee in the krypton ionization yield at this intensity [34]. Interestingly, the

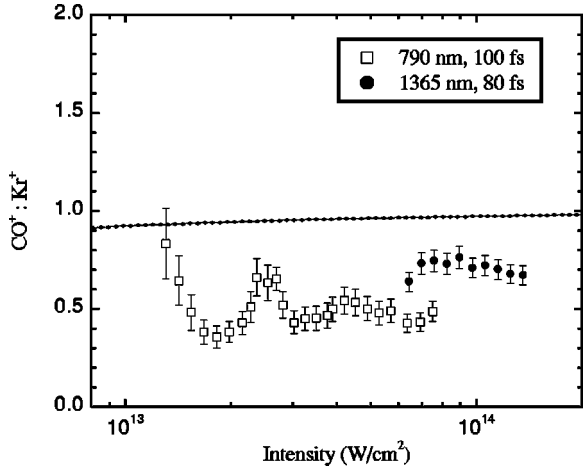

FIG. 9. The measured ratio of CO^+ to Kr^+ as a function of laser intensity. The solid line is an ADK calculation for 790 nm, 100 fs pulses; the dashed line is the same calculation but for 1365 nm, 80 fs pulses. Both wavelengths are focused with the 5 cm mirror.

CO:Kr ratio is slightly less than that of N_2:Ar or F_2:Ar. While the ratio of molecular to atomic ionization in the latter targets is above 1.0, in the former case it is roughly one half. This suppression, however, is insignificant compared to that observed for O_2, D_2, S_2, and SO. Note that we also performed measurements with 1365 nm radiation, where CO is in the tunneling regime, and obtained a similar ratio.

To our knowledge, the only readily available diatomic molecule that does not have either a singlet or triplet ground state is NO. This molecule has a doublet ground state and a low IP. We compared it to a xenon target, since, as for S_2 and SO, no easily accessible companion atom was available. At

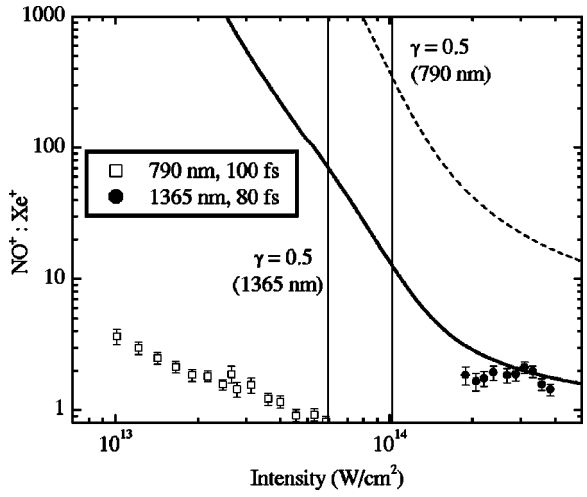

FIG. 10. The measured ratio of NO^+ to Xe^+ as a function of laser intensity. Two calculations are shown: 1365 nm, 80 fs pulses focused with a 5 cm mirror (solid line); and 790 nm, 100 fs pulses focused by a 30 cm lens (dashed line). As in Fig. 2, the vertical lines mark the intensities where $\gamma = 0.5$ for the indicated wavelengths. The tunneling calculation is in agreement with the measured 1365 nm data near saturation; however, the slopes of the data and of the calculation disagree significantly.

1365 nm (see Fig. 10) the measured ratio was between 1.0 and 2.0, indicating that NO was slightly suppressed, given the 2.9 eV difference in ionization potentials. When $NO^+:Xe^+$ is compared to the ADK prediction at 2×10^{14} W/cm^2, the measured value is $\sim 1.5\times$ smaller than the model calculation. This amount of suppression is less than that observed for S_2 and SO in similar comparisons to ADK theory. At lower wavelength (790 nm) and intensity, the ratio ranged from a value of 1.5 to nearly 4. Even considering the rapid increase in the ratio at low intensities, the experimental result is considerably below the prediction of the ADK theory.

It is difficult to reconcile all of the above data with any particular model of intense field ionization of diatomic molecules. Given the success of the interference model [26] in describing O_2 and N_2 ionization rates, it is reasonable to assume that the interference model has merit. Indeed, a similar interference effect has recently been observed in ionizing ion-molecule collisions [57]. We note, however, that the collisional effect [57] is far more subtle than the ionization suppression observed in this and previous work. Of course, the collision experiment [57] used hydrogen molecules as a target, and the calculations [26] were performed for F_2, N_2, and O_2. The fact that the model is unable to correctly describe the S_2 or F_2 behavior might indicate that, in these targets, there are other molecular effects that are at least equally as important.

The structure model [25] invokes an effective charge and ionization potential based on the amount of screening provided to the outer electron by the inner electrons. The arguments made by Guo [25] for O_2 are easily extended to S_2 and SO, since they have similar electronic structure. As previously noted, however, the antisymmetric wave function of F_2 is similar to O_2 as well, and no suppression is observed in this case. Finally, the charge screening effect that is the essence of the structure model cannot be applied to D_2. So, while these additions to tunneling theory provide more accurate results in some cases, they do not seem generally applicable.

In lieu of a satisfactory theoretical description, we offer the following observations regarding our experimental results. First, with the notable exception of D_2, there seems to be some relation between the ground-state wave function symmetry and the ionization rate. Molecules with singlet ground states ionize at rates roughly comparable to rare-gas targets of similar IP. Molecules with triplet states, however, appear to be more difficult to ionize. All of the triplet molecules measured (O_2, S_2, and SO) are from $5\times$ to $30\times$ harder to ionize than expected, based on the predictions of the ADK theory (SO and S_2) or on measured rates in a companion atom of similar IP (O_2:Xe). In contrast, the ionization yields of singlet N_2, F_2, and CO are within a factor of 2 of their companion atoms. Doublet NO seems to fall in the middle, showing slight suppression for the 1365 nm data, and significant suppression for the 790 nm data when compared to ADK predictions. The exception to this trend is H_2 (D_2). The difference between the equilibrium internuclear distance in the neutral molecule and the molecular ion, however, is unique among the targets studied. The result of

this difference is that the vertical IP of H_2 (D_2) is quite different from the IP calculated by subtracting the difference in ground-state energies of D_2 and D_2^+ (IP_0). While IP_0 is lower for H_2 (D_2) than for Ar (see Table I), the vertical IP is actually higher (see Fig. 6). In the other molecules considered, the difference between the vertical and ground-state IPs is much smaller. It is quite possible, therefore, that hydrogen molecules must be viewed as a special case when considering their ionization yields as compared to atomic targets of similar IP.

Second, suppression, or lack thereof, seems to be relatively independent of the wavelength of the ionizing radiation over the range of wavelengths in this measurement. This would indicate that the differences in atomic and molecular ionization rates are not specific to the multiphoton or tunneling mechanisms.

Third, our measured ratios are often fairly constant over a range of laser intensities until the ionization threshold is reached for one target, at which point the ratio rapidly rises or falls. This behavior is quite unexpected. While tunneling theory predicts unity rate ratios for species with identical IPs, it also predicts highly intensity-dependent ratios for species with different IPs.

Fourth, molecules with lower IPs are generally suppressed. This is also unexpected, since ADK theory tends to underestimate the ionization yield of both molecular and atomic targets in the region where $\gamma > 0.5$ and multiphoton ionization becomes more prevalent (see Refs. [20,25] for examples). Thus, when comparing a molecular target of 9 or 10 eV to xenon (IP = 12.13 eV), the ADK calculation is expected to yield a molecular:atomic ratio that is smaller than one would expect if the multiphoton contribution could be included. Nevertheless, SO, S_2, and NO are all suppressed relative to the expectations of ADK theory. Conversely, with the exception of D_2, molecular targets with higher IPs (N_2, F_2, and CO) display molecular:atomic ionization yield ratios similar to the predictions of ADK calculations.

Finally, heteronuclear molecules seem, in general, slightly harder to ionize than homonuclear molecules of similar electronic properties. CO, unlike N_2 and F_2, is slightly more difficult to ionize than its companion atom. Furthermore, while S_2, O_2, and SO are all suppressed, SO is the most suppressed of these three electronically similar species.

IV. SUMMARY

In summary, we have used the ratiometric ionization measurement method to make accurate comparisons of the ionization yields of molecules and atoms. We have used this technique to explore the ionization behavior of most readily available diatomic molecules. While simple SAE based models of molecular ionization describe the gross properties observed, our experimental results have demonstrated that the problem of accurately predicting molecular ionization behavior is more difficult than has been previously assumed. Modifications of existing atomic models are not sufficient to describe the details of differences between molecular and atomic targets. In general, we find that molecules in singlet configurations display more atomlike ionization properties, while doublet or triplet configurations appear to have suppressed ionization rates relative to an atomic target of similar IP. Hydrogen molecules are an exception to this rule, but this might be accounted for by the difference in the equilibrium internuclear distance of the neutral and molecular ion. We hope that these results will stimulate further theoretical examination of the basic process of strong-field molecular interaction.

ACKNOWLEDGMENTS

This work was supported by the Chemical Sciences, Geosciences and Biosciences Division, Office of Basic Energy Sciences, Office of Science, U.S. Department of Energy, by the Packard Foundation, and by the National Science Foundation IGERT program under Grant No. MPS-9972790.

[1] K. J. Schafer and K. C. Kulander, Phys. Rev. A **42**, 5794 (1990).
[2] K. C. Kulander, K. J. Schafer, and J. L. Krause, in *Atoms in Intense Laser Fields*, edited by M. Gavrila (Academic Press, New York, 1992).
[3] H. G. Muller and F. C. Kooiman, Phys. Rev. Lett. **81**, 1207 (1998).
[4] M. J. Nandor, M. A. Walker, L. D. Van Woerkom, and H. G. Muller, Phys. Rev. A **60**, R1771 (1999).
[5] A. Becker, L. Plaja, P. Moreno, M. Nurhuda, and F. H. M. Faisal, Phys. Rev. A **64**, 023408 (2001).
[6] A. Becker and F. H. M. Faisal, Phys. Rev. Lett. **84**, 3546 (2000).
[7] A. Assion, T. Baumert, M. Bergt, T. Brixner, B. Kiefer, V. Seyfried, M. Strehle, and G. Gerber, Science **282**, 919 (1998).
[8] R. J. Levis, G. M. Menkir, and H. Rabitz, Science **292**, 709 (2001).
[9] C. W. S. Conover, E. Wells, M. J. DeWitt, and R. R. Jones (unpublished).
[10] M. J. DeWitt *et al.*, Chem. Phys. **218**, 211 (1997).
[11] S. M. Hankin, D. M. Villeneuve, P. B. Corkum, and D. M. Rayner, Phys. Rev. Lett. **84**, 5082 (2000).
[12] S. M. Hankin, D. M. Villeneuve, P. B. Corkum, and D. M. Rayner, Phys. Rev. A **64**, 013405 (2001).
[13] F. H. M. Faisal, J. Phys. B **6**, L89 (1973).
[14] H. R. Reiss, Phys. Rev. A **22**, 1786 (1980).
[15] L. V. Keldysh, Sov. Phys. JETP **20**, 1307 (1965).
[16] A. M. Perelomov, V. S. Popov, and M. V. Terent'ev, Sov. Phys. JETP **23**, 924 (1966).
[17] M. V. Ammosov, N. B. Delone, and V. P. Krainov, Sov. Phys. JETP **64**, 1191 (1986).
[18] S. L. Chin *et al.*, J. Phys. B **25**, L249 (1992); T. D. G. Walsh, *et al.*, *ibid.* **26**, L85 (1993); **27**, 3767 (1994).
[19] A. Talebpour, C.-Y. Chien, and S. L. Chin, J. Phys. B **29**, L677 (1996).
[20] C. Guo, M. Li, J. P. Nibarger, and G. N. Gibson, Phys. Rev. A **58**, R4271 (1998).

[21] A. Talebpour, S. Larochelle, and S. L. Chin, J. Phys. B **31**, L49 (1998).
[22] K. P. Huber and G. Herzberg, in *NIST Chemistry WebBook, NIST Standard Reference Database 69*, edited by P. J. Linstrom and W. G. Mallard (National Institute of Standards and Technology, Gaithersburg, MD, 2001), http://webbook.nist.gov
[23] M. J. DeWitt and R. J. Levis, J. Chem. Phys. **108**, 7739 (1998).
[24] A. Saenz, J. Phys. B **33**, 4365 (2000).
[25] C. Guo, Phys. Rev. Lett. **85**, 2276 (2000).
[26] J. Muth-Böhm, A. Becker, and F. H. M. Faisal, Phys. Rev. Lett. **85**, 2280 (2000).
[27] F. H. M. Faisal and A. Becker, in *Selected Topics on Electron Physics*, edited by D. M. Campbell and H. Kleinpoppen (Plenum, New York, 1986), p. 397; F. H. M. Faisal, A. Becker, and J. Muth-Böhm, Laser Phys. **9**, 115 (1999).
[28] F. Grasbon *et al.*, Phys. Rev. A **63**, 041402(R) (2001).
[29] J. Muth-Böhm, A. Becker, S. L. Chin, and F. H. M. Faisal, Chem. Phys. Lett. **337**, 313 (2001).
[30] V. R. Bhardwaj, D. M. Rayner, D. M. Villeneuve, and P. B. Corkum, Phys. Rev. Lett. **87**, 253003 (2001).
[31] M. J. DeWitt, E. Wells, and R. R. Jones, Phys. Rev. Lett. **87**, 153001 (2001).
[32] P. Hansch *et al.*, Phys. Rev. A **54**, R2559 (1996); P. Hansch and L. D. VanWoerkom, Opt. Lett. **21**, 1286 (1996).
[33] I. Ben-Itzhak *et al.*, J. Phys. B **34**, 1143 (2001).
[34] H. Maeda, M. Dammasch, U. Eichmann, W. Sandner, A. Becker, and F. H. M. Faisal, Phys. Rev. A **62**, 035402 (2000).
[35] S. F. J. Larochelle, A. Talebpour, and S. L. Chin, J. Phys. B **31**, 1201 (1998); **31**, 1215 (1998).
[36] A. Talebpour, C.-Y. Chien, Y. Liang, S. Larochelle, and S. L. Chin, J. Phys. B **30**, 1721 (1997).
[37] W. C. Wiley and I. H. McLaren, Rev. Sci. Instrum. **26**, 1150 (1955).
[38] Stanford Research Systems, RGA 200/2, Sunnyvale, CA.
[39] R. C. Wetzel *et al.*, Phys. Rev. A **35**, 559 (1987).
[40] R. S. Freund, R. C. Wetzel, and R. J. Shul, Phys. Rev. A **41**, 5861 (1990).
[41] M. V. V. S. Rao and S. K. Srivastava, J. Phys. B **29**, 1841 (1996).
[42] E. Krishnakumar and S. K. Srivastava, Int. J. Mass Spectrom. Ion Processes **113**, 1 (1992).
[43] D. Rapp and P. Englander-Golden, J. Chem. Phys. **43**, 1464 (1964).
[44] Y.-K. Kim *et al.*, J. Chem. Phys. **106**, 1026 (1997).
[45] J. Berkowitz and W. A. Chupka, J. Chem. Phys. **40**, 287 (1964).
[46] J. Berkowitz and C. Lifshitz, J. Chem. Phys. **48**, 4346 (1968).
[47] W. Mroz, D. Fry, M. P. Stöckli, and S. Winecki, Nucl. Instrum. Methods Phys. Res. A **447**, 335 (1999).
[48] W. Mroz, M. P. Stöckli, D. Fry, A. Prokopiuk, and B. Walch, Rev. Sci. Instrum. **71**, 1100 (2000).
[49] V. Mergal, *Dynamische Elektron Korrelation in Helium* (Shaker-Verlag, Aachen, 1996).
[50] R. Dörner *et al.*, Phys. Rev. Lett. **76**, 2654 (1996).
[51] E. Wells, Ph.D. thesis, Kansas State University, Manhattan, KS, 2000.
[52] R. Dörner *et al.*, Phys. Rep. **330**, 95 (2000).
[53] M. J. DeWitt and R. J. Levis, J. Chem. Phys. **108**, 7739 (1998).
[54] M. J. Frisch *et al.*, computer code GAUSSIAN 98 (revision A.9), (Gaussian, Inc., Pittsburgh, PA, 2001).
[55] A. Becker, A. D. Bandrauk, and S. L. Chin, Chem. Phys. Lett. **343**, 345 (2001).
[56] Note that our ADK calculations simply use the static (with the exception of the D_2 calculation discussed in Sec. III C) molecular IP instead of an atomic IP, and the rate is determined in the same manner as for a single atom. This is done for comparison purposes only (i.e., to determine the amount of suppression), and we do not wish to imply that this is a correct method for obtaining a molecular ionization rate.
[57] N. Stolterfoht *et al.*, Phys. Rev. Lett. **87**, 023201 (2001).